

Thermal Analyses of a Human Kidney and a Rabbit Kidney During Cryopreservation by Vitrification

Lili E. Ehrlich

Department of Mechanical Engineering,
Carnegie Mellon University,
Pittsburgh, PA 15213

Gregory M. Fahy

21st Century Medicine, Inc.,
Fontana, CA 92336

Brian G. Wowk

21st Century Medicine, Inc.,
Fontana, CA 92336

Jonathan A. Malen

Department of Mechanical Engineering,
Carnegie Mellon University,
Pittsburgh, PA 15213

Yoed Rabin¹

Department of Mechanical Engineering,
Carnegie Mellon University,
Pittsburgh, PA 15213
e-mail: rabin@cmu.edu

This study focuses on thermal analysis of the problem of scaling up from the vitrification of rabbit kidneys to the vitrification of human kidneys, where vitrification is the preservation of biological material in the glassy state. The basis for this study is a successful cryopreservation protocol for a rabbit kidney model, based on using a proprietary vitrification solution known as M22. Using the finite element analysis (FEA) commercial code ANSYS, heat transfer simulations suggest that indeed the rabbit kidney unquestionably cools rapidly enough to be vitrified based on known intrarenal concentrations of M22. Scaling up 21-fold, computer simulations suggest less favorable conditions for human kidney vitrification. In this case, cooling rates below -100°C are sometimes slower than $1^{\circ}\text{C}/\text{min}$, a rate that provides a clear-cut margin of safety at all temperatures based on the stability of rabbit kidneys in past studies. Nevertheless, it is concluded in this study that vitrifying human kidneys is possible without significant ice damage, assuming that human kidneys can be perfused with M22 as effectively as rabbit kidneys. The thermal analysis suggests that cooling rates can be further increased by a careful design of the cryogenic protocol and by tailoring the container to the shape of the kidney, in contrast to the present cylindrical container. This study demonstrates the critical need for the thermal analysis of experimental cryopreservation and highlights the unmet need for measuring the thermophysical properties of cryoprotective solutions under conditions relevant to realistic thermal histories. [DOI: 10.1115/1.4037406]

Keywords: cryopreservation, vitrification, kidney, thermal analysis, computer simulation

Introduction

Organ cryopreservation is being increasingly recognized as an important problem of human medicine due to its theoretical ability to substantially improve both the logistics and outcomes of transplantation [1,2]. Whereas it may be possible to preserve some organs successfully by freezing [3–6], others, such as the kidney, appear to require cryopreservation by vitrification [7,8] in which the formation of ice is avoided and instead, the organ is preserved in a noncrystalline, glassy state [9–11]. For vitrification to be successful, very high concentrations of cryoprotective agents (CPAs) must be used compared to the concentrations needed for freezing protocols. Unfortunately, such high concentrations introduce the risk of serious toxicity and significantly complicate the introduction and removal of the cryoprotectant [12]. Recently, many of the problems associated with cryoprotecting the rabbit kidney have been solved adequately to enable vitrification without loss of viability [13,14], but it remains to be seen whether these solutions translate well to vitrification of much larger organs.

In this paper, we address this question by using thermal modeling and information about the stability of the amorphous state to simulate and predict the vitrification of both rabbit and human kidneys. Modeling is advantageous in view of the difficulty and cost of acquiring real human and large animal organs for vitrification studies. Modeling tools can be applied to an organ of any geometry and size, creating a highly efficient way to plan for and reduce the needed number of actual experiments. Moreover, recent advances in the characterization of thermal properties of CPAs during vitrification [15,16] have made such modeling more realistic than ever before.

The essential problem of vitrifying the kidney is that it is a highly heterogeneous organ. Whereas it is easy to ensure extreme stability of the amorphous state in the renal cortex, it is difficult to do so in the renal inner medulla [7,12,13]. For example, full saturation of the cortex would confer it with a critical cooling rate (CCR) of $0.1^{\circ}\text{C}/\text{min}$ or less [17]. A medullary concentration of only 92.1% of full-strength M22, as previously reported [7], will require a higher cooling rate to avoid ice formation, but the exact cooling rates required have not previously been well defined. In the present study, we derive more specific information about the relationship between M22 concentration and the CCR, which is necessary for the thermal analysis of the system.

The objective of this study is to investigate the thermal conditions associated with cryopreservation by vitrification in a kidney model. This study focuses on the cooling portion of the cryopreservation protocol, from tissue loading with the CPA solution to cryogenic storage. The investigated thermal protocol is adopted from a prior experimental investigation on a rabbit kidney model. The same thermal protocol is further investigated on a 21-fold larger system containing a human kidney. This study is based on computer simulations using the finite element analysis (FEA) approach and the ANSYS commercial code.

Materials and Methods

Physical Model. A geometrical model of a human kidney was downloaded from the NIH three-dimensional Print Exchange [18]. This model is based on computed tomography imaging, which was further made water tight for FEA simulations in this study. The kidney model was scaled to have a volume of 209 ml, which is average for an adult human male [19].

Figure 1(a) displays a realistic illustration of a human kidney in a cylindrical CPA container. Figure 1(b) displays a schematic

¹Corresponding author.

Manuscript received April 14, 2017; final manuscript received July 7, 2017; published online October 26, 2017. Assoc. Editor: Ram Devireddy.

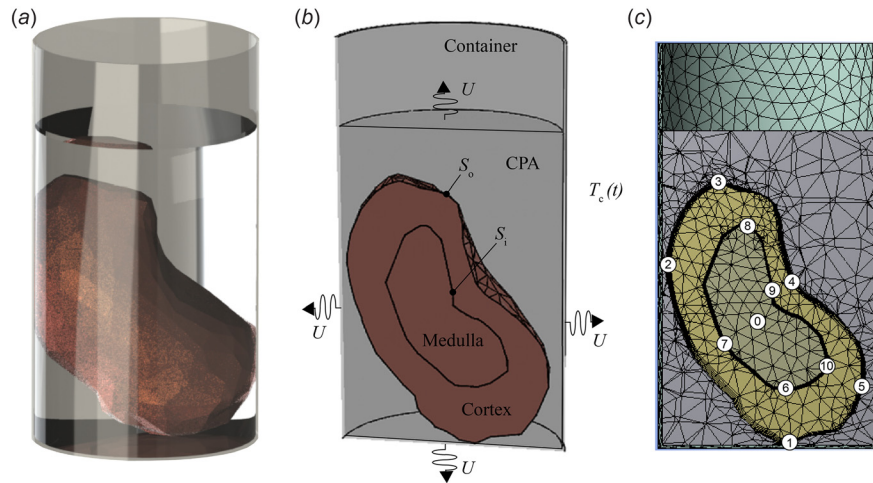


Fig. 1 Illustrations of system analyzed in this study: (a) a kidney in a cylindrical container filled with CPA; (b) schematic view of the four subdomains of the system, each characterized by unique thermal properties; heat transfer processes and material properties of the constituents; and (c) a cross section of the system showing the FEA mesh and virtual thermal sensors

illustration of a cross section of the system, highlighting its four subdomains: renal medulla, renal cortex, contained CPA, and container. While the cylindrical container geometry allows simplicity in simulations, it is also advantageous for generating a relatively uniform volumetric heating effect at the rewarming stage by applying a radiofrequency (RF) electrical field [20]. The overall volume of the container was selected to be practical for the chosen kidney size. The physical properties of the cylindrical container were selected to be similar to those of commercial cryobags, as listed in Table 1. Specifically, a cylindrical container having the following dimensions can contain a human kidney: an inner diameter of 8.9 cm, a height of 16.3 cm, and a wall thickness of 1.1 mm. These dimensions permit complete immersion of the kidney down to 2.1 cm below the CPA level, while the container wall extends 3.5 cm above the CPA level for handling purposes. The container is assumed to be uncovered during cooling, exposing the surface of the CPA to the same forced convection cooling conditions as the container walls and base. With this geometry, the container accommodates 581 ml of CPA in addition to the kidney volume. From thermal considerations, the portion of the wall extending above the CPA level bears negligibly on the analysis.

The geometrical model of the rabbit kidney is simply a scaled-down version of the human kidney to an overall volume of 9.8 ml, in order to meet previous experimental parameters [7] while maintaining geometric similarity. This assumption is deemed appropriate since the rodent kidney has a similar cortical volume fraction as the human kidney and the internal structure of the rodent kidney is similar to that of the rabbit kidney [33]. While the cortex of a rodent kidney resembles that of a human kidney, the internal anatomy of the medulla is quite different between humans and rodents. Nevertheless, since the heat transfer simulation is dominated by the CPA fraction and its thermophysical properties, while ignoring the detail of the medullary anatomy, the latter difference is assumed to have no effect on the simulation outcome. The rabbit kidney container volume was selected to be compatible with a shortened Thermo Scientific Nalgene 6250-9050 sample vial, used previously in unpublished rabbit kidney vitrification studies. The scaled-down container model had the following dimensions: an inner diameter of 3.2 cm, a height of 5.9 cm, and a wall thickness of 0.4 mm. With this geometry, the container accommodates 27 ml of CPA in addition to the rabbit kidney volume.

Table 1 Material properties used in the current study, where temperature-dependent properties are presented in °C within the range of −22 °C to −135 °C

Material	Thermal conductivity, k ($\text{W m}^{-1} \text{ }^\circ\text{C}^{-1}$)	Specific heat, C_p ($\text{J kg}^{-1} \text{ }^\circ\text{C}^{-1}$)	Density, ρ (kg m^{-3})
Fresh human kidney—cortex	0.503 [21]	3941 ^a	1049 [22]
Fresh human kidney—medulla	0.503 [21]	3908 ^a	1044 [22]
Fresh rabbit kidney—cortex	0.465–0.490 (76.6–79.8% water) [23]	3772 ^{a,b}	—
Fresh rabbit kidney—medulla	0.502–0.544 (82.0–86.0% water) [23]	3772 ^{b,c}	—
Nonaqueous components of human kidney ^c	0.260	2732 ^{a,b,c}	—
M22	$0.316 + 7.13 \times 10^{-5}T - 1.26 \times 10^{-5}T^2 - 1.47 \times 10^{-7}T^3 - 4.75 \times 10^{-10}T^4$ [24]	—	1080 (unpublished)
7.05 M DMSO	$0.356 + 7.42 \times 10^{-4}T - 1.29 \times 10^{-6}T^2 - 6.87 \times 10^{-8}T^3 - 2.95 \times 10^{-10}T^4$ [15]	$2804 + 4.205T - 0.0547T^2 - 4.9027T^3$ [25]	$1058 - 0.417T$ [26]
Ice	$2.22 - 1.0 \times 10^{-2}T + 3.45 \times 10^{-5}T^2$ [27]	$2066 + 6.9T$ [27]	$917 - 0.11T$ [27]
Water at 4.4 °C	0.575 [28]	4208 [28]	999.8 [28]
Low-density polyethylene—container	$0.14 - 1.3 \times 10^{-4}T$ [29]	$1121 + 3.94T$ [30]	$1055 - 0.267T$ [31]

^aCompiled based on the EMT [32] using 80% water and 20% nonaqueous components.

^bCompiled from thermal conductivity and thermal diffusivity data [21] assuming overall density of 1000 kg/m³.

^cAverage property for the entire kidney.

Thermal History. The thermal history in this theoretical study follows successful experimental investigations on rabbit kidneys using the CPA cocktail M22 [7]. In this past work, bare kidneys that had been loaded with M22 solution by perfusion ending at a temperature of -22°C were placed in a Linde BF1 biological freezer for cooling by fan-driven cold vapor from injected liquid nitrogen. The measured thermal history from that experimental study [6] is replicated in the present simulation study. Unlike past experimental work, the present analysis includes a container, which is necessary for RF rewarming and future clinical application.

The thermal history of a complete organ vitrification experiment as modeled here includes seven key stages: (i) precooling the container and contained CPA down to -50°C ; (ii) precooling of the kidney down to -22°C during M22 perfusion; (iii) dropping the precooled kidney into the precooled CPA container; (iv) cooling the container at a rapid rate down to the storage temperature of -135°C ; (v) holding the entire system at the storage temperature for as long as needed; (vi) rewarming the system by means of RF energy up to -22°C ; and (vii) washing out the M22 by perfusion and recovering the organ. The current study focuses on the cooling and storage portion of the protocol (including stages (iii), (iv), and thermal equilibration in stage (v)), with the cooling chamber thermal history marked with a dashed line as T_c in Fig. 2.

During the cooling process, an overall heat transfer coefficient of $350\text{ W/m}^2\text{ }^{\circ}\text{C}$ is assumed between the outer surfaces of the

container and the cooling chamber temperature, as specified in Fig. 2. The same heat transfer coefficient is also assumed at the CPA air surface. Although measured in a different system, the previously mentioned heat transfer coefficient value is assumed typical to a controlled-rate cooler, when the air inside the cooling chamber is well mixed [25]. Note that Feig et al. [25] have experimentally validated the application of ANSYS for solving the heat conduction problem during vitrification under conditions similar to those presented in the current study. Further note that for such a high heat transfer coefficient by convection as of $350\text{ W/m}^2\text{ }^{\circ}\text{C}$, the cooling rate in the domain is essentially dominated by conduction (Biot number > 10). Finally, note that the heat transfer coefficient by convection in the chamber can be easily elevated, by air flow constrictions for example [34], while the intrinsic properties of thermal conductivity (or, alternatively, thermal diffusivity for the purpose of discussion) cannot be altered without modifying the CPA, which makes this property a limiting factor for the cooling rates necessary for vitrification.

Heat Transfer Model. Heat transfer within the organ-CPA-container system is assumed to be solely by conduction

$$\rho_j C_{p,j} \frac{\partial T_j}{\partial t} = \nabla \cdot (k_j \nabla T_j) \quad (1)$$

where ρ is the density, C_p is the specific heat, T is the temperature, t is the time, k is the thermal conductivity, and j is the subdomain index, standing for either the cortex, medulla, CPA solution, or container wall. Continuity in temperature and heat flux are assumed on all internal boundaries between the subdomains of the system. Heat convection in the CPA solution is assumed negligible in the current analysis due to the high viscosity of the solution at the starting temperature of -50°C [12].

The heat transfer between the external system boundaries and the mixed air within the cooling chamber is

$$-k_j \frac{\partial T_j}{\partial \hat{n}} = U(T_j - T_c) \quad (2)$$

where \hat{n} is the normal to the system's outer surface and U is the overall heat transfer coefficient, combining the effects of convection and thermal radiation.

Thermal Properties. The objective in the current study is twofold: (i) to investigate whether a specific cryogenic cooling protocol ensures complete vitrification in a rabbit kidney model and (ii) to investigate if the same protocol is expected to yield similar results in a human kidney model. The approach taken in this study is to investigate the envelope conditions, rather than to investigate a wide selection of special cases. The base case analyzed in this study is of a completely vitrified system, where latent heat effects are absent, and for which thermophysical properties are readily available (Table 1). In particular, thermal conductivity data on relevant vitrified CPA cocktails have been recently developed [16,24] and are included in the current study (Table 1).

An additional case is investigated where complete vitrification is also assumed, but for which water ice thermophysical properties are taken instead of the vitrified CPA properties. The rationale for this specific investigation is to explore the errors that such material properties selection might lead to—a repeated practice in theoretical studies in the absence of specific data. This special case is not simulative of partial crystallization as the latent heat effect is not included. A partially vitrified material will display midrange thermophysical properties between the amorphous and the icelike state. Such properties could be first-order approximated using the effective medium theory (EMT), based on the constituent volume fractions and properties of the primitive ingredients [32].

Consistent with prior experimental studies [7,12], the properties of M22 are selected for the vitrified CPA. Four limiting cases are

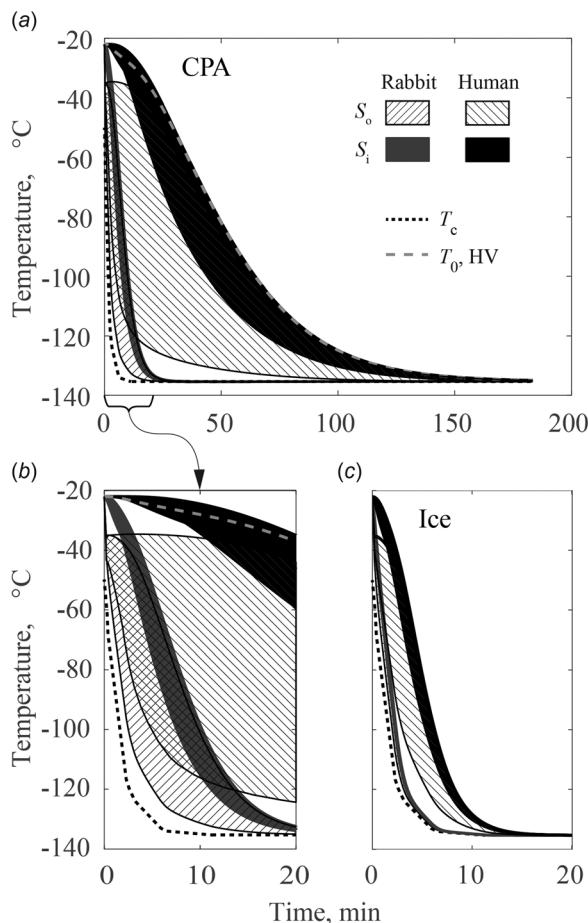


Fig. 2 Thermal history in the kidney model for (a) a vitrified system with CPA properties, (b) the same system at the early stage of cooling, and (c) a vitrified system but with ice properties, where S_o is the outer surface of the cortex, S_i is the medulla–cortex interface, T_c is the temperature of the cooling chamber, and T_0 is the temperature at the center of the kidney (Fig. 1(c))

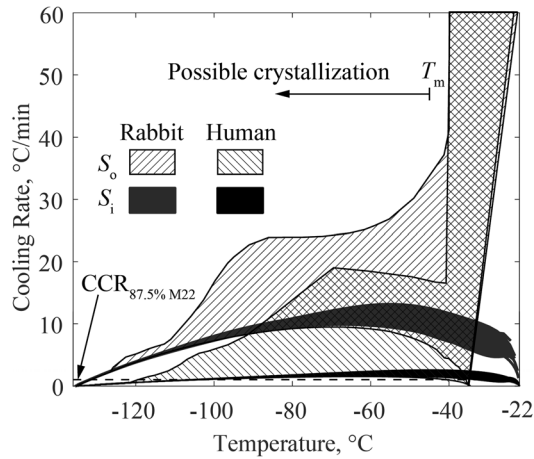


Fig. 3 Cooling-rate history in the vitrified kidney model, where S_o is the outer surface of the cortex, S_i is the medulla–cortex interface (Fig. 1(c)), and CCR_{med} is the CCR for 87.5% M22 in the medulla ($1^\circ\text{C}/\text{min}$)

investigated in this study: a fully vitrified rabbit kidney model using CPA properties (RV) and water ice properties (RI), and a fully vitrified human kidney model using CPA properties (HV) and using water ice properties (HI).

The specific thermophysical properties used in this study are listed in Table 1, including low-density polyethylene as a container material for cryogenic temperatures. It can be seen from Table 1 that water occupies roughly 78% of the rabbit kidney cortex and 82% of the rabbit kidney medulla. During vitrification, the entire kidney is approximated as having the same thermal conductivity as the pure CPA solution for the following reasons: (i) the thermal conductivity of the nonaqueous components of the tissue differs by only 18% from that of M22 at 0°C as compiled by the EMT theory ($0.31\text{ W/m}^\circ\text{C}$ for M22 and $0.26\text{ W/m}^\circ\text{C}$ for the nonaqueous material [21]); (ii) the thermal conductivity of vitrified M22 varies by only 10% over the temperature range of -135°C and 0°C (from $0.28\text{ W/m}^\circ\text{C}$ to $0.31\text{ W/m}^\circ\text{C}$, respectively) [24]; and, (iii) data are unavailable to compile the thermal conductivity of the nonaqueous components of the tissue at cryogenic temperatures.

While the specific heat monotonically decreases with decreasing temperature, the sudden change in its rate at the glass transition temperature is neglected in this study for simplicity in calculations. The glass transition temperature, T_g , for M22 is -123°C , which is about 11°C above the storage temperature in this study, and has a minimal effect on energy removal during cooling.

A reference solution of 7.05 M dimethyl sulfoxide (DMSO) is also listed in Table 1, which has served well in previous studies of thermomechanical stresses in cryopreservation [26,35]. The difference in thermal conductivity between vitrified M22 and vitrified 7.05 M DMSO is 5.2% at -22°C and 3.5% at -135°C , which is within the range of experimental uncertainties [15,24]. Due to the similarity in thermal conductivity characteristics and since the specific heat for M22 is unavailable, the specific heat of 7.05 M DMSO is assumed to apply for the present vitrified system.

Ice Formation Tendency in Dilutions of M22. While the medulla and the cortex are approximated to have the same thermal properties due to their high CPA concentrations, a small deviation in actual concentration may affect significantly the CCR needed to ensure vitrification. Nearly 100% of the full concentration of M22 is expected to be reached in the renal cortex, conferring a CCR of $0.1^\circ\text{C}/\text{min}$ and possibly even slower [17]. However, we

wanted to verify that a typical, previously reported medullary concentration of just 92.1% of the full concentration of M22 [7] would have a CCR slower than $1^\circ\text{C}/\text{min}$, as previously inferred [7]. Once verified, a cooling rate of $1^\circ\text{C}/\text{min}$ would be taken as an indication of vitrification success in the thermal analysis in this study.

We therefore undertook a differential scanning calorimetry investigation to determine the threshold concentration that ensures vitrification at a cooling rate of at least $1^\circ\text{C}/\text{min}$. Dilutions of M22 in its standard carrier solution LM5 [10] were cooled at $1^\circ\text{C}/\text{min}$ from -22°C down to -90°C , below which further ice growth is inhibited by high solution viscosity [36]. Samples were then warmed from -90°C back to -22°C at $160^\circ\text{C}/\text{min}$, while searching for the melting peak heat flux on the differential scanning calorimetry output as an indication of any ice that formed. This rapid warming rate is beneficial for instrument sensitivity and avoidance of ice growth during warming.

In increments of 2.5% in concentration, this investigation revealed that, at a cooling rate of $1^\circ\text{C}/\text{min}$, 1.27% w/w ice formed in 85% M22 and 0.085% w/w ice formed in 87.5% M22. Using the Boutron convention of a 0.2% w/w ice threshold as the criterion for defining the CCR [34], the concentration of M22 that will remain vitreous at a cooling rate of $1^\circ\text{C}/\text{min}$ is about 87.5% of full M22. This concentration threshold is lower by 5.1% than the 92.1%-of-full-M22 concentration previously reported to be achieved in the inner medulla of a rabbit kidney that survived indefinitely after vitrification, rewarming, and transplantation [6]. The critical cooling rate of 92.1% M22 is clearly $\ll 1^\circ\text{C}/\text{min}$ and too slow to easily measure. This indicates that if cooling rates on the order of $1^\circ\text{C}/\text{min}$ can be achieved in human kidneys, there is no question that they can be vitrified successfully.

Numerical Solution. The FEA commercial code ANSYS was used to simulate heat conduction in the system, with the element mesh displayed in Fig. 1(c). Due to geometrical complexity, the CPA solution and the kidney were meshed using tetrahedral (SOLID87) and hexahedral (SOLID90) elements based on an ANSYS meshing algorithm. Program-controlled inflation was used during mesh generation, with finer discretization at the interface between the medulla and the cortex, and at the outer surface of the cortex. In total, 49,197 elements were used in the case of the human kidney and 26,231 elements were used in the case of the rabbit kidney, which satisfied a mesh convergence analysis for the thermal solution.

Eleven numeric labels are displayed in Fig. 1(c), simulating strategically placed virtual temperature sensors for the purpose of thermal analysis. In general, one sensor is placed at the geometric center of the kidney, five sensors on the outer surface of the kidney (surface S_o), and five on the interface between the medulla and the cortex (surface S_i). The specific sensor locations are (0) the geometric center of the kidney, (1) the point of contact between kidney cortex and the base of the container, (2) the point of contact between the kidney cortex and the container wall, (3) the highest point on S_o , (4) the closest point on S_o to the geometric center of the system (11.5 mm and 8.4 mm apart for the human case and rabbit case, respectively), (5) the farthest point on S_o from point 2 in the horizontal direction, (6) the lowest point on S_i , (7) the farthest point on S_i from the geometric center of the system, (8) the highest point on S_i , (9) the closest point on S_i to the geometric center of the system (5.4 mm and 4.8 mm apart for the human case and rabbit case, respectively), and (10) the closest point on S_i to point 5 in the horizontal direction. The thermal histories collected from those virtual sensors were used to determine the instantaneous variations in temperature and in cooling rate, as discussed later.

The numerical solution was executed from the time of kidney immersion in the precooled M22 and down to the storage temperature of -135°C . At the time of immersion, the initial temperature of the kidney was -22°C , while the temperature of the

precooled M22 in the container was -50°C . Thermal equilibrium at cryogenic storage was assumed after the slowest responding point in the kidney conformed to 99.5% of the overall change in kidney temperature, which equals -134.4°C (the kidney is cooled from -22°C to -135°C during the simulation). A time-step convergence study for the FEA yielded a time-step value of 12.5 s for numerical simulations.

Results and Discussion

Figure 2 displays the thermal history in the cooling chamber, T_c , the thermal history at the geometric center of the kidney, T_0 , and the thermal history range on surfaces S_o and S_i , as compiled from the outputs of the virtual sensors presented in Fig. 1(c). Close inspection of FEA results at all mesh nodes confirmed that, indeed, those sensors capture the temperature range along the respective surfaces, although different sensors may display extreme values at different times. As can be expected, the temperature distribution within the kidney becomes less uniform with the increasing size of the system. The system containing the human kidney is 21 times larger than the system containing the rabbit kidney.

The sudden immersion of the kidney in a surrounding CPA solution at the onset of cooling leads to a steplike temperature change on the surface of the kidney, S_o (from -22°C to -50°C). The result of this sudden temperature drop is not fully captured graphically in the time scale relevant to Fig. 2, where almost instantaneously the surface temperatures drop to about -36°C —the average initial temperatures of the kidney and the surrounding CPA solution. The propagation of thermal information from that surface is measured in a much longer time scale, which is proportional to the thermal diffusivity (the ratio of thermal conductivity to the volumetric specific heat).

A significantly longer period of time is required for the vitrified systems to approach steady-state (defined by 99.5% response; see Numerical Solution section for further discussion). For the cases presented in Fig. 2, the RV and HV cases required 25.8 min and 176.7 min to approach the steady-state respectively, while the RI and HI cases required only 9.8 and 15.4 min to approach a steady-state, respectively. The significantly different results of the RV/HV cases from the RI/HI cases underscore the importance of using thermal properties of the specific CPA solution for vitrification simulations, rather than attempting to approximate them as similar to those of ice.

In general, the significant differences between an amorphous CPA system and a crystallized water system bound the range of thermal conductivity values for the case of a partially vitrified system [15]. Nonetheless, due to the high CPA concentration, partially vitrified solutions will exhibit properties closer to those of a completely vitrified system [16]. Furthermore, when a partially vitrified system is under consideration, one must bear in mind that crystallization may be spatially nonuniform and further dependent upon the local thermal history and the stochastic presence of local nucleation events and concentration fluctuations. This means that partial vitrification scenarios must be investigated on a case-by-case basis. Fortunately, due to the relatively low CCR of M22 and its relatively slow kinetics of crystallization [17], the outcome from any practical case of partial kidney vitrification will likely be much closer to the outcomes of the RV and HV cases.

It can be seen from Fig. 2 that the temperature distribution on the outer surface of the kidney, S_o , is less uniform than the temperature distribution on S_i . Comparing the differences in temperature ranges between S_i and S_o with the temperature differences between T_0 and S_i indicates steeper temperature gradients across the cortex. More generally, the wide temperature ranges displayed in Fig. 2 highlight the difficulty in temperature measurements in experimental studies when only one or a few sensors are attached to the outer surface of the kidney. This difficulty intensifies with increased organ size. It follows that several strategically placed sensors are required to determine the thermal history in kidney

experiments, where their strategic locations can be informed by numerical simulations.

Figure 3 displays the cooling-rate history at the center of the kidney and the respective cooling-rate ranges on surfaces S_o and S_i . Recall that the sudden immersion of the kidney (initially at -22°C) in the surrounding CPA solution (initially at -50°C) leads to a rapid kidney surface cooling immediately after immersion (Fig. 2). Consequently, it warms up the surrounding CPA solution above its initial temperature of -50°C , while the temperature of the cooling chamber hosting the container continues to decrease according to its preset controlled thermal history. Shortly thereafter, the entire surrounding CPA solution is cooled again below -50°C , eventually leading to thermal equilibrium at the storage temperature. This effect of initial warming of the surrounding CPA solution while the temperature of the cooling chamber keeps dropping leads to an adverse effect of diminished cooling rates close to the surface at the early stage of the process, when the kidney surface temperature is about -36°C (recall, the initial temperature average of the precooled surrounding CPA and the perfused kidney).

Fortunately, the above sudden decrease in cooling rates takes place above the melting temperature for 90% M22, which is -45°C [37]. By the time that any local temperature in the kidney reaches -45°C , its corresponding cooling rate is already above $1^{\circ}\text{C}/\text{min}$, which is higher than the CCR for the solution concentrations under consideration ($\geq 92.1\%$, see “Materials and Methods” section). For reference, the minimum cooling rate anywhere in the human kidney at -45°C , -75°C , -100°C , and -123°C is $1.2^{\circ}\text{C}/\text{min}$, $1.5^{\circ}\text{C}/\text{min}$, $1.5^{\circ}\text{C}/\text{min}$, and $0.4^{\circ}\text{C}/\text{min}$, respectively.

Counterintuitively and quite seriously, if the initial temperature of the surrounding CPA were lower than -50°C , it is possible that the local cooling rate at some portion of the kidney would drop below the CCR and some extent of harmful ice crystals may form at higher temperatures. For example, an initial surrounding CPA solution temperature of -90°C would result in subcritical cooling rate near the surface of the kidney when it almost instantaneously reaches the average temperature of -55°C —the melting temperature, T_m , of 100% concentration M22. Note that the maximum crystal growth rate is observed at temperatures closer to the melting temperature, while the maximum ice nucleation rate is found closer to the glass transition temperature [37]. The latter effect is not easy to infer from visualization of physical events in large specimens [25,36].

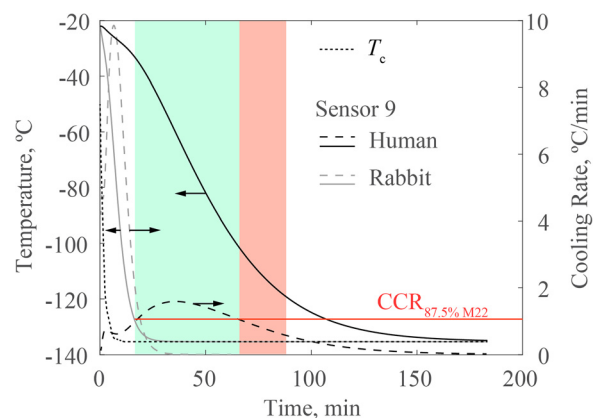


Fig. 4 Thermal history of sensor 9 (the closest point in the medulla to center of system) for the cases of a vitrified human kidney and a vitrified rabbit kidney. The colored areas refer to the human kidney simulation, where green (left highlighted area) corresponds to the time range in which the sensor indicates temperatures below T_m and the cooling rate is above the CCR of 87.5% M22, while red (right highlighted area) corresponds to the time range in which the sensor indicates temperatures above T_g and the cooling rate is below CCR of 87.5% M22; colored areas interface at -103°C (between the left and right highlighted areas).

While the adverse effect of initial surrounding CPA solution temperature on rewarming can be reduced by a careful thermal design of the process and its specialized hardware, it signifies the need for computer simulations in the design of the cryopreservation protocol. Given the obtained cooling rates and the dependency of the CCR on the CPA solution concentration, results of this study farther signify the critical need to design means for improved CPA solution substitution in the organ. The possibility of marginal cooling rates at some portion of the kidney also signifies the need for detailed modeling of the thermophysical properties. Measurement of physical properties during partial vitrification represents a relatively uncharted area of research [15,16,26,38,39].

Figure 4 displays the thermal history at sensor 9, which is the closest to the geometric center of the system (5.4 mm and 4.8 mm from the center for the human and rabbit kidney, respectively). While the cooling rate for the rabbit kidney (RV) case exceeds, the CCR within the relevant temperature range of T_m to T_g , the human kidney (HV) case shows subcritical cooling rates between -103°C and T_g . Figure 5 displays the temperature fields in the cross section of the kidney for the HV case when the same sensor temperature indicates -30°C , -60°C , -90°C , and -120°C . The respective cooling rates at the same location at the corresponding points in time are $0.8^\circ\text{C}/\text{min}$, $1.6^\circ\text{C}/\text{min}$, $1.3^\circ\text{C}/\text{min}$, and $0.5^\circ\text{C}/\text{min}$.

It can be observed from Fig. 4 that the cooling rate at sensor 9 falls below the desired $1^\circ\text{C}/\text{min}$ in the temperature range of -103°C and T_g , where the nucleation rate is the highest. It can further be seen from Fig. 4 that the cooling rate at sensor 9 is

always below $-1.6^\circ\text{C}/\text{min}$, which is relatively close to the preferred limit of $-1^\circ\text{C}/\text{min}$ in the medulla.

The observations reported here could be taken to suggest that the vitrification of a human kidney could be marginal given that the CCR for 87.5% M22 is not always attained during all phases of cooling. However, the CCR for 92.1% M22 is considerably lower, and that concentration is known to be achievable at least in the rabbit kidney. Furthermore, although the CCR is defined without regard to the temperature dependence of the CCR, in fact, damaging ice formation is only possible at relatively high temperatures ($>-90^\circ\text{C}$) during cooling. Thus, cooling rates that only fall below the nominal CCR at very low temperatures, when the CPA viscosity is high enough to inhibit ice growth, need not preclude successful vitrification during cooling. However, long cooling times between -100°C and T_g promote nucleation of large numbers of new ice crystals on the nanoscale. Although stable and innocuous at low temperature, these ice nuclei complicate later recovery of the organ by requiring warming rates faster than the CCR to minimize their growth during passage through warmer temperatures favorable for ice growth. The difficulties of warming successfully are expected to worsen with increasing time spent between -100°C and T_g , where the ice nucleation rate is maximum, although the magnitude of the effect has not been determined. As Mehl has pointed out [9–11], ice nuclei formed near T_g tend to all be the same size and to grow at the same rate upon warming, which means that a warming rate sufficient to limit a few ice crystals to innocuous sizes may be sufficient to limit many ice crystals to innocuous sizes.

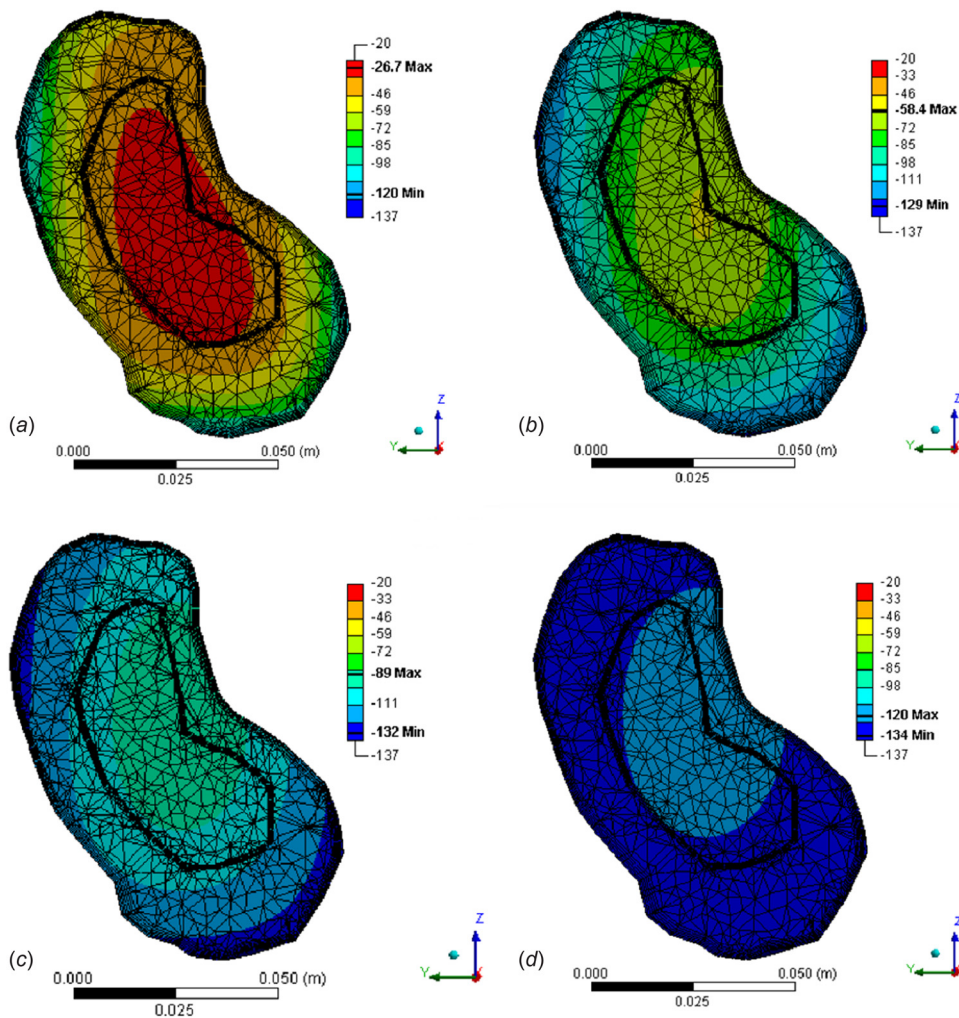


Fig. 5 Temperature fields when the sensor 9 indicates (a) -30°C , (b) -60°C , (c) -90°C , and (d) -120°C

Additional steps can be taken to reduce the likelihood of crystallization in the kidney on cooling. The most important of these is to maximize the concentration of M22 in the medulla, and recent innovations have made this possible [13,14]. From a thermal engineering point of view, another option is to reduce the overall volume of the container while tailoring it to the shape of the kidney, which will decrease the overall heat capacity of the system (heat capacity being the product of specific heat and mass) and hence accelerate cooling. Since the kidney mass is only about 1/4 of the entire system, the scope for improving the average cooling rate in this way is significant. By the same token, the CPA solution surrounding the kidney can slow down later rewarming, but this effect could also be reduced by using computer simulations to optimize the design of the cryopreservation equipment. However, RF rewarming may add additional constraints on the container shape, which are beyond the scope of the current study.

Summary and Conclusions

Thermal analyses of a rabbit kidney and a human kidney are presented in this study, subject to conditions that have proven successful in vitrification experiments on a rabbit model. This study is based on computer simulations using the FEA commercial code ANSYS. An adult human male kidney model is used in this study and analyzed in a cylindrical container suitable for radiofrequency rewarming. The rabbit kidney model is essentially a 21-fold scaled-down version of the human kidney to meet previous experimental parameters [7]. This study integrates newly generated data on the CCR for M22 concentrations relevant to kidney cryopreservation, where M22 is a proprietary CPA cocktail successfully used in previous experiments, and criteria for vitrification success are obtained with at least 5% concentration margins.

Results of this study demonstrate that the temperature distribution within the kidney becomes significantly less uniform when the system is scaled up from a rabbit size to a human size. Consistently, the cooling-rate distribution increases with the increasing size of the kidney, and yet even in the case of the human kidney, cooling rates remain high enough in all parts of the kidney to prevent ice formation at temperatures above -100°C . This was observed despite the fact that the volume modeled in the case of human kidney was 21-fold larger than that modeled in the case of the rabbit kidney. Nevertheless, it would still be desirable to reduce the overall volume of the kidney container, particularly by tailoring it to the shape of the kidney. The thermal design of optimal kidney packaging is left for future studies.

In conclusion, this study demonstrates the value of thermal design and analysis of cryopreservation protocols using computer simulations. This study further highlights the unmet need for measuring the thermophysical properties of the CPA solutions in the relevant thermal histories. In particular, several strategically placed sensors may be required to determine the thermal outcome in kidney experiments due to variations in thermal history across the organ to be informed by numerical simulations.

Acknowledgment

This study has been supported in parts by Award No. R01HL127618 from the National Heart Lung and Blood Institute. The content is solely the responsibility of the authors and does not necessarily represent the official views of the National Heart Lung and Blood Institute or the National Institutes of Health. This work has also been funded in part by the Dowd Fellowship from the College of Engineering at Carnegie Mellon University. The authors would like to thank Philip and Marsha Dowd for their financial support and encouragement.

Funding Data

- Dowd Fellowship, College of Engineering, Carnegie Mellon University.

References

- [1] Giwa, S., 2017, "The Promise of Organ and Tissue Preservation to Transform Medicine," *Nat. Biotechnol.*, **35**(6), pp. 530–542.
- [2] Lewis, J. K., Bischof, J. C., Braslavsky, I., Brockbank, K. G. M., Fahy, G. M., Fuller, B. J., Rabin, Y., Tocchio, A., Woods, E. J., Wovk, B. G., Acker, J. P., and Giwa, S., 2016, "The Grand Challenges of Organ Banking: Proceedings From the First Global Summit on Complex Tissue Cryopreservation," *Cryobiology*, **72**(2), pp. 169–182.
- [3] Campbell, B. K., Hernandez-Medrano, J., Onions, V., Pincott-Allen, C., Aljaser, F., Fisher, J., McNeilly, A. S., Webb, R., and Picton, H. M., 2014, "Restoration of Ovarian Function and Natural Fertility Following the Cryopreservation and Autotransplantation of Whole Adult Sheep Ovaries," *Hum. Reprod.*, **29**(8), pp. 1749–1763.
- [4] Dittrich, R., Maltaris, T., Mueller, A., Dimmler, A., Hoffmann, I., Kiesewetter, F., and Beckmann, M. W., 2006, "Successful Uterus Cryopreservation in an Animal Model," *Horm. Metab. Res.*, **38**(3), pp. 141–145.
- [5] Hamilton, R., Holst, H. I., and Lehr, H. B., 1973, "Successful Preservation of Canine Small Intestine by Freezing," *J. Surg. Res.*, **14**(4), pp. 313–318.
- [6] Wang, Z., He, B., Duan, Y., Shen, Y., Zhu, L., Zhu, X., and Zhu, Z., 2014, "Cryopreservation and Replantation of Amputated Rat Hind Limbs," *Eur. J. Med. Res.*, **19**(1), p. 28.
- [7] Fahy, G. M., Wovk, B., Pagotan, R., Chang, A., Phan, J., Thomson, B., and Phan, L., 2009, "Physical and Biological Aspects of Renal Vitrification," *Organogenesis*, **5**(3), pp. 167–175.
- [8] Jacobsen, I. A., Pegg, D. E., Starklind, H., Chemnitz, J., Hunt, C., Barfort, P., and Diaper, M. P., 1984, "Effect of Cooling and Warming Rate on Glycerolized Rabbit Kidneys," *Cryobiology*, **21**(6), pp. 637–653.
- [9] Fahy, G. M., and Wovk, B., 2015, "Principles of Cryopreservation by Vitrification," *Cryopreservation and Freeze-Drying Protocols*, W. F. Wolkers, and H. Oldenhof, eds., Springer, New York, pp. 21–82.
- [10] Fahy, G. M., MacFarlane, D. R., Angell, C. A., and Meryman, H. T., 1984, "Vitrification as an Approach to Cryopreservation," *Cryobiology*, **21**(4), pp. 407–426.
- [11] Wovk, B., 2010, "Thermodynamic Aspects of Vitrification," *Cryobiology*, **60**(1), pp. 11–22.
- [12] Fahy, G. M., Wovk, B., Wu, J., Phan, J., Rasch, C., Chang, A., and Zendejas, E., 2004, "Cryopreservation of Organs by Vitrification: Perspectives and Recent Advances," *Cryobiology*, **48**(2), pp. 157–178.
- [13] Fahy, G., 2013, "041 Consequences and Control of Ice Formation in the Renal Inner Medulla," *Cryobiology*, **67**(3), pp. 409–410.
- [14] Fahy, G. M., 2016, "Elimination of Most Damage After Perfusing Rabbit Kidneys With M22 Solutions," *Cryobiology*, **73**(3), p. 407.
- [15] Ehrlich, L. E., Feig, J. S. G., Schiffes, S. N., Malen, J. A., and Rabin, Y., 2015, "Large Thermal Conductivity Differences between the Crystalline and Vitrified States of DMSO With Applications to Cryopreservation," *PLoS One*, **10**(5), p. e0125862.
- [16] Ehrlich, L. E., Malen, J. A., and Rabin, Y., 2016, "Thermal Conductivity of the Cryoprotective Cocktail DP6 in Cryogenic Temperatures, in the Presence and Absence of Synthetic Ice Modulators," *Cryobiology*, **73**(2), pp. 196–202.
- [17] Wovk, B., and Fahy, G. M., 2005, "Toward Large Organ Vitrification: Extremely Low Critical Cooling and Warming Rates of M22 Vitrification Solution," *Cryobiology*, **51**, p. 362.
- [18] NIH, 2017, "Heart, Aorta and Kidney CAD Model—NIH 3D Print Exchange," National Institutes of Health, Rockville, MD, accessed Dec. 12, 2016, <https://3dprint.nih.gov/discover/3dpx-000906>
- [19] Cheong, B., Muthupillai, R., Rubin, M. F., and Flamm, S. D., 2007, "Normal Values for Renal Length and Volume as Measured by Magnetic Resonance Imaging," *Clin. J. Am. Soc. Nephrol.*, **2**(1), pp. 38–45.
- [20] Evans, S., 2000, "Electromagnetic Rewarming: The Effect of CPA Concentration and Radio Source Frequency on Uniformity and Efficiency of Heating," *Cryobiology*, **40**(2), pp. 126–138.
- [21] Valvano, J. W., Cochran, J. R., and Diller, K. R., 1985, "Thermal Conductivity and Diffusivity of Biomaterials Measured With Self-Heated Thermistors," *Int. J. Thermophys.*, **6**(3), pp. 301–311.
- [22] Duck, F. A., 2013, *Physical Properties of Tissues: A Comprehensive Reference Book*, Academic Press, London.
- [23] Holmes, K. R., Ryan, W., and Chen, M. M., 1983, "Thermal Conductivity and H₂O Content in Rabbit Kidney Cortex and Medulla," *J. Therm. Biol.*, **8**(4), pp. 311–313.
- [24] Ehrlich, L. E., Malen, J. A., and Rabin, Y., 2016, "Thermal Conductivity of M22," (unpublished).
- [25] Feig, J. S. G., Solanki, P. K., Eisenberg, D. P., and Rabin, Y., 2016, "Polarized Light in Scanning Cryomicroscopy—Part II: Thermal Modeling and Analysis of Experimental Observations," *Cryobiology*, **73**(2), pp. 272–281.
- [26] Rios, J. L. J., and Rabin, Y., 2006, "Thermal Expansion of Blood Vessels in Low Cryogenic Temperatures—Part II: Vitrification With VS55, DP6, and 7.05 M DMSO," *Cryobiology*, **52**(2), pp. 284–294.
- [27] Fukusako, S., 1990, "Thermophysical Properties of Ice, Snow, and Sea Ice," *Int. J. Thermophys.*, **11**(2), pp. 353–372.
- [28] Holman, J., 2009, *Heat Transfer*, McGraw-Hill Education, Boston, MA.
- [29] Zhang, X., Hendro, W., Fujii, M., Tomimura, T., and Imaishi, N., 2002, "Measurements of the Thermal Conductivity and Thermal Diffusivity of Polymer Melts With the Short-Hot-Wire Method," *Int. J. Thermophys.*, **23**(4), pp. 1077–1090.
- [30] Gaur, U., and Wunderlich, B., 1982, "Heat Capacity and Other Thermodynamic Properties of Linear Macromolecules. V. Polystyrene," *J. Phys. Chem. Ref. Data*, **11**(2), pp. 313–325.

- [31] Patnode, W., and Scheiber, W. J., 1939, "The Density, Thermal Expansion, Vapor Pressure, and Refractive Index of Styrene, and the Density and Thermal Expansion of Polystyrene," *J. Am. Chem. Soc.*, **61**(12), pp. 3449–3451.
- [32] Wang, J., Carson, J. K., North, M. F., and Cleland, D. J., 2006, "A New Approach to Modelling the Effective Thermal Conductivity of Heterogeneous Materials," *Int. J. Heat Mass Transfer*, **49**(17–18), pp. 3075–3083.
- [33] Giraud, S., Favreau, F., Chatauret, N., Thuillier, R., Maiga, S., and Hauet, T., 2011, "Contribution of Large Pig for Renal Ischemia-Reperfusion and Transplantation Studies: The Preclinical Model," *J. Biomed. Biotechnol.*, **2011**, p. 532127.
- [34] Boutron, P., 1993, "Glass-Forming Tendency and Stability of the Amorphous State in Solutions of a 2,3-Butanediol Containing Mainly the Levo and Dextro Isomers in Water, Buffer, and Euro-Collins," *Cryobiology*, **30**(1), pp. 86–97.
- [35] Rabin, Y., and Plitz, J., 2005, "Thermal Expansion of Blood Vessels and Muscle Specimens Permeated With DMSO, DP6, and VS55 at Cryogenic Temperatures," *Ann. Biomed. Eng.*, **33**(9), pp. 1213–1228.
- [36] Feig, J. S. G., Eisenberg, D. P., and Rabin, Y., 2016, "Polarized Light Scanning Cryomacroscopy—Part I: Experimental Apparatus and Observations of Vitrification, Crystallization, and Photoelasticity Effects," *Cryobiology*, **73**(2), pp. 261–271.
- [37] Wowk, B., 2007, "Ice Nucleation and Growth in Concentrated Vitrification Solutions," *Cryobiology*, **55**(3), p. 330.
- [38] Eisenberg, D. P., Taylor, M. J., and Rabin, Y., 2012, "Thermal Expansion of the Cryoprotectant Cocktail DP6 Combined With Synthetic Ice Modulators in Presence and Absence of Biological Tissues," *Cryobiology*, **65**(2), pp. 117–125.
- [39] Jimenez Rios, J. L., and Rabin, Y., 2006, "Thermal Expansion of Blood Vessels in Low Cryogenic Temperatures—Part I: A New Experimental Device," *Cryobiology*, **52**(2), pp. 269–283.